2025 IEEE/SICE International Symposium on System Integration (SII)
January 21-24, 2025, Munich, Germany

A Data-driven Comparison of Resistive-Viscoelastic Models for a 3D-Printed Conductive Solid

Sourajit Mukherjee and Takeshi Takaki* *Member, IEEE*

***Abstract*— Conductive polymer composites with piezoresistive properties have found extensive use in force sensing applications, such as strain gauges. Polylactic acid filled with carbon black nano-fillers is one such easily available and inexpensive material. The piezoresistive properties of conductive polymers have been shown to share an equivalence with the linear viscoelastic relationship between stress and strain. In this study, we examine six progressively complex resistive-viscoelastic models based on this relationship. After empirically determining the model parameters, we compared their stress prediction outputs using resistance data as input, which had been recorded while subjecting a 3D-printed conductive solid to a compressive force. We observed the model performances for two cases: when model parameters are determined from the complete test cycle and when they are determined phase-wise. Phase-wise coefficients showed a much better prediction accuracy and it was also observed that simpler models gave a better performance than more complex models.**

I. Introduction

Conductive Polymer composites (CPCs) have huge potential in the manufacture of intrinsically sensitive parts and are fast becoming the preferred way of 3D printing piezoresistive sensors. Generally, a CPC is made of an insulating polymer matrix embedded with conductive particles made of metals, various forms of carbon, or semiconductors like silica. CPC-based sensors can be made of materials such as multiwalled carbon nanotubes and polydimethylsiloxane composite (MWCNT/PDMS), conductive acrylonitrile butadiene styrene (ABS) filled with carbon black (CB), polylactic acid (PLA) filled with carbon nanotubes (CNT), etc.

Due to the multi-phase composite nature of CPCs, which combine a flexible polymer matrix and an inelastic filler, the stiffness of the material is usually lower than the pure polymer itself due to higher porosity [1]. However, plastics are generally much easier to manufacture into complex designs than metals. Hence, the advantage of conductive plastics cannot be ignored. The CPC used in this study – composite conductive PLA, is made of regular PLA embedded with Carbon-Black nanoparticle fillers. It displays behavior similar to viscoelastic solids. The stress-strain relation of such materials falls in between a Hookean elastic solid and a Newtonian viscous fluid [2]. Hence, the behavior of a general viscoelastic body is described by combining springs, dashpots, and other elements into a rheological model for lumped parameter analysis. Two of the most fundamental rheological models for viscoelastic bodies combine a single spring and a single dashpot element. The Maxwell body is modelled as a spring and damper in series and closely resembles the behavior of thermoplastics, while the Kelvin body is modelled as a spring and damper in parallel and resembles thermosets. However, these models are not sufficiently complex to describe the behavior of real bodies. In 1997, Kamath and Wereley [3] proposed a model for electrorheological fluids that combined the pre-yield viscoelastic behavior with the post-yield viscous behavior using a non-linear hyperbolic shape function. They modeled the viscoelastic behavior with a 3-parameter fluid model using a viscous element in series with a Kelvin element. The standard 3-parameter model for solids, also called a Zener model, however, uses a spring in series with a Kelvin element or a spring in parallel with a Maxwell element. Kalantari *et al*. [4] used a Kelvin-Zener model to determine the electromechanical behavior of Linqstat, a carbon-filled polyethylene which is a semiconductive viscoelastic solid. They utilized percolation theory and a Kelvin-Zener mechanical model to predict the force acting on the material based on the change in resistance. This model was also adopted by Yong and Aw [5] to characterize the behavior of a carbon black/silicon elastomer composite. In 2019, Wang *et al*. [6] derived a simplified model for relating the pressure applied to a CPC-based metal filled piezoresistor, with the consequent change in relative resistance using the percolation theory. Guo *et al*. [7] used a Maxwell-Zener model to partially represent the equivalent electro-mechanical behavior of a MWCNT/PDMS composite strain sensor, by deriving a relationship between relative resistance and the material's elastic moduli. Subsequently, four-parameter models which use a Maxwell element in series with a Kelvin element (Kelvin representation) or two parallel Maxwell elements (Maxwell representation) have also been widely studied by academicians. Burger's model, as it is commonly known, was used by Paredes-Madrid *et al*. [8] in their statistical study on the creep response of CPCs under dynamic loading. On the other hand, Garzon-Hernandez *et al*. [9] used a 4-parameter constitutive model with a friction plate element to simulate 3D-printed solids. To further extend the complexity, generalized rheological models have also been developed, for example if multiple branches of Maxwell elements with different spring and damper constants are in parallel with a spring element, known as the Weichert model. Mu *et al*. [10] used the generalized Weichert model to characterize the behavior of silver wires printed using a silver nanoparticle-based ink. They showed

This work was supported by COI-NEXT (Bio-Digital Transformation) and JST SPRING, Grant Number JPMJSP2132.

*Corresponding Author, takaki@hiroshima-u.ac.jp
First Author: sourajitm10@gmail.com
At the time of writing, all authors are part of the Smart Robotics Lab, Graduate School of Advanced Science and Engineering, Hiroshima University, Hiroshima, Japan

that the resistance relaxation of CPCs can be modeled using an electrical equivalent of the mechanical rheological model, and presented a relation between the relative resistance and applied strain. Gao *et al*. [11] used a similar idea to show the relationship between resistance relaxation and strain of a CPC is similar to the one between strain and stress. They used a 2nd order Zener model (two Zener models in parallel) to establish this relationship for fabric-based resistive sensors, while Kouchakzadeh and Narooei [12] concluded that the behavior of ABS and TPU-based CPCs show a very good agreement with the hyperelastic and hyper-viscoelastic models respectively. Kadival *et al*. [13] evaluated the efficacy of an artificial neural network (ANN) generated model of viscoelastic behavior against generalized Maxwell and Peleg models and found the ANN model gave a close fit to the predictions of the other two. Karabal and Yildiz [14] observed the effect of using carbon black to reinforce the mechanical behavior of high performance polyetherimide (PEI) and modeled the creep behavior using Burger's rheological model and Findley's power law equation.

Considering that the electrical behavior of a CPC shares an equivalence with its mechanical behavior, it can be gathered that the stress-resistance relationship can be modeled similar to stress-strain. In this study, we present a data-based analysis and compare the efficacy of several stress prediction models, established using the idea of observed electro-mechanical equivalence. Using the recorded force and voltage values for a 3D-printed solid, obtained from a uniaxial compression test, we numerically estimate the constant coefficients for the constitutive equations of each model for two case-studies. First, we estimate the values over an entire test-cycle. Then, we estimate the values separately for each phase, i.e., the loading phase and the unloading phase. We compare the closeness of the stress v/s time profile predicted by each model for the two case studies, to determine the most appropriate model applicable for solids 3D printed with conductive PLA.

Section II details the specifics of the experimentation and data collection, such as the materials and test equipment used. Section III is dedicated to the mathematical background and a brief explanation of the coefficient estimation algorithm. Section IV discusses the results of stress prediction using the various models and Section V presents our concluding remarks on this study.

II. Testing and Setup

A. Test Specifications

The experiment in this study was done on a specimen printed with PLA/CB. The material was acquired in a 3D-printable filament form from 'Protopasta', with a filament diameter of 1.75mm. It is a composite made of 'Natureworks' 4043D PLA as the matrix, a dispersant and filled with conductive carbon black nanoparticles [15]. It has a density of 1.15 g/cm^3.

Schematic of the test setup is shown in Fig. 1. The specimen was printed with a size which was adjusted according to the size of the compression head (a circular surface on the loading end with a diameter of 60 mm) and maximum loading capacity of the force tester. The manufactured specimen was mounted on a non-conductive polyacetal fixture, bolted to a raised solid stainless-steel platform. The polyacetal block was drilled with holes at appropriate locations to securely fix the specimen in the center. A desktop force tester, 'MCT-2150' (A&D Ltd.) was used for conducting the tests. It has a maximum loading capacity of 500N and minimum testing speed of 10mm/min. The specimen was clamped on top of the polyacetal fixture and subjected to a single-cycle compression test with the load varying from 0N to a maximum of 450N, at a loading speed of 10mm/min. The body of the specimen was printed with

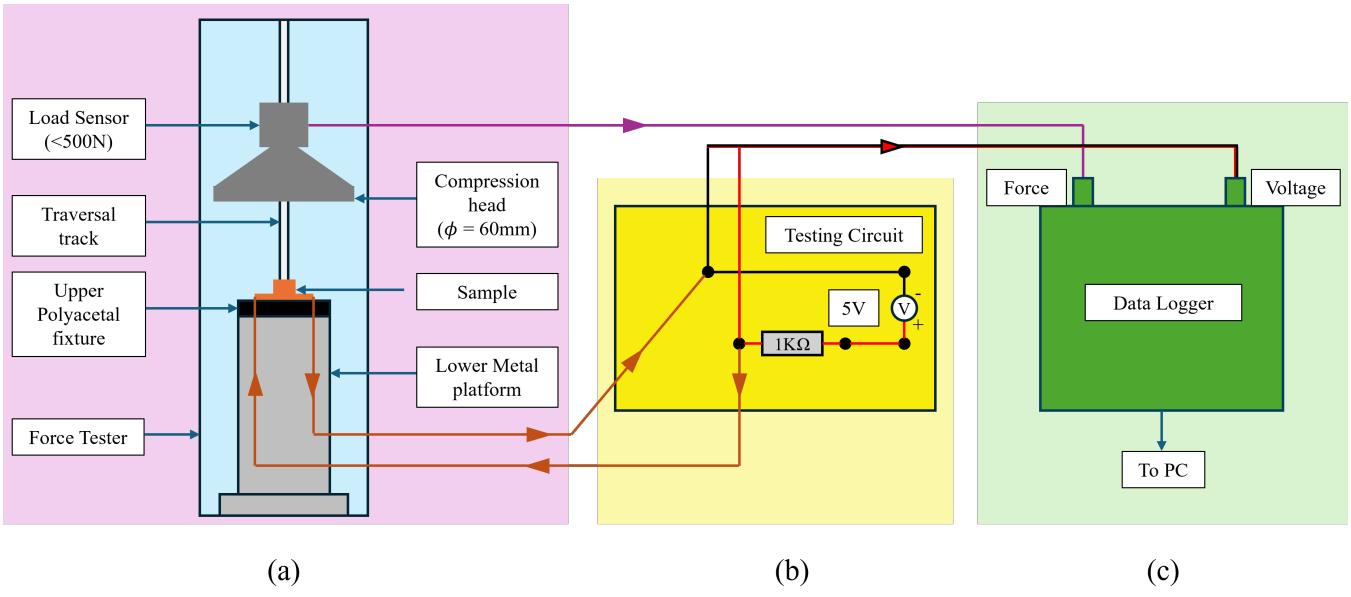

Fig. 1. The test setup schematic (a) Force Tester and Test bed (Front View) (b) Testing circuit (c) Data Logger

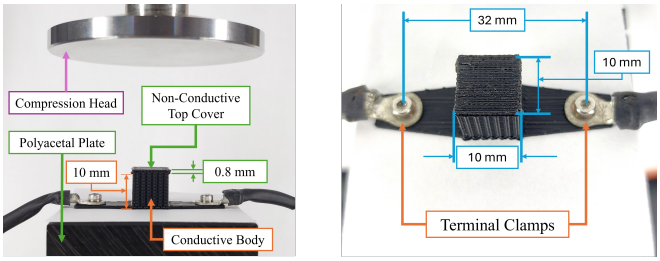

(a) (b)

Fig. 2. The printed specimen used for testing (a) Front View (b) Top View

protruding terminals from opposite edges at the bottom, which were connected to the testing circuit using ring terminals. Both terminals were fixed onto the polyacetal block with M2 bolts to hold the specimen in place. The supply voltage was set at 5.0 V.

B. Specimen Design

The specimen for testing was printed using the 'QIDI Tech i-fast' printer. Table-I shows the printing parameters used. The conductive body of the specimen was printed as a cube of side 10 mm, with an infill of 50%. Four additional layers of regular PLA were printed on top of the conductive part in order to prevent conduction through the metal compression head on contact. The plane of the layers of the printed cube were oriented horizontally during testing, i.e., perpendicular to the axis of compression. The printed specimen is shown in Fig. 2. The terminals protruding from the conductive body were printed at the bottom, so they acted as both connectors and clamps.

C. Data Collection and Analysis

Force and voltage data were collected through the data logger 'Kyowa PCD-430A' as shown in Fig. 1(c), using its data-logging software 'DCS-100'. All the data was recorded at 10 Hz and is saved in '*.csv' files. 'MathWorks MATLAB' was used to further process and analyze the data.

The force values were converted into engineering stress by dividing it with the area of the sample in mm^2. Similarly, the voltage values were used to calculate the equivalent resistance of the specimen at each time-step, by using the voltage divider formula. This resistance is further normalized by converting into relative resistance, $\mathcal{R}$:

$$\mathcal{R} = \frac{R - R_0}{R_0}$$

Hence, $\mathcal{R}$ is the normalized change in resistance $(R - R_0)$ of the specimen over its initial resistance, R_0.

TABLE I
PRINTING PARAMETERS FOR THE SPECIMEN

Setting	Value
Filament Diameter	1.75mm
Infill Pattern	Line
Infill Percentage	50%
Track Direction(s)	[0°, 90°]
Number of Shells	0
Layer Height	0.2mm
Extrusion Width	0.4mm
Nozzle Size	0.4mm
Printing Temperature	230 °C
Build Plate Temperature	60 °C

III. Resistive Viscoelastic Modeling and Parameter Estimation

A. Mathematical Models

Based on the percolation theory of conduction in polymers, it is agreed that there exists a non-linear relationship between resistance and strain [6], [16]. However, for low strain deformations (< 0.1), applicable for this study, the relationship appears to be linear. Considering this, strain has been directly substituted with relative resistance in the constitutive equations of several existing rheological models, allowing us to calculate stress directly from the measured relative resistance. The generalized constitutive viscoelastic stress-strain relation can be expressed as a standard ordinary differential equation with constant coefficients[17]:

$$\sigma + \sum_{k=1}^{n} p_k \frac{d^k \sigma}{dt^k} = \sum_{k=0}^{n} q_k \frac{d^k \varepsilon}{dt^k} \tag{1}$$

Where, σ is uniaxial stress, ε is the uniaxial strain and t is time. The value of coefficients p_k and q_k will depend on the

TABLE II
RESISITIVE-VISCOELASTIC MODELS CHOSEN FOR COMPARISON

Model Name	Equation	
Hooke	$\sigma = q_0 \mathcal{R}$	(2)
Maxwell	$\sigma + p_1 \dot{\sigma} = q_1 \dot{\mathcal{R}}$	(3)
Kelvin	$\sigma = q_0 \mathcal{R} + q_1 \dot{\mathcal{R}}$	(4)
Zener	$\sigma + p_1 \dot{\sigma} = q_0 \mathcal{R} + q_1 \dot{\mathcal{R}}$	(5)
Burger	$\sigma + p_1 \dot{\sigma} + p_2 \ddot{\sigma} = q_1 \dot{\mathcal{R}} + q_2 \ddot{\mathcal{R}}$	(6)
Generalized Kelvin (2 units)	$\sigma + p_1 \dot{\sigma} = q_0 \mathcal{R} + q_1 \dot{\mathcal{R}} + q_2 \ddot{\mathcal{R}}$	(7)

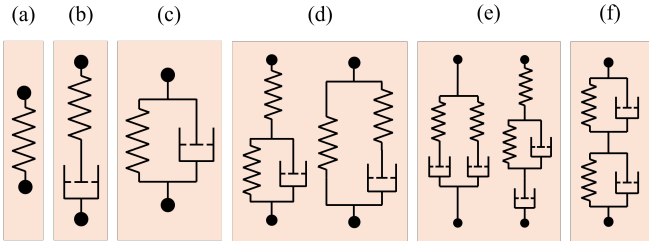

Fig. 3. The selected Rheological models (a) 1-Parameter Hooke's Model (b) 2-Parameter Maxwell model (c) 2-Parameter Kelvin Model (d) 3-Parameter Zener models (e) 4-Parameter Burger's models (f) Generalized Kelvin Model with 2 Kelvin Units / 4-Parameter Kelvin Model

model being considered and are constant forb the purposes of this study. Table-II gives the generalized resistive-viscoelastic equations derived from (1), considered for evaluation in this study.

In (1), the numerical subscripts of the coefficient indicates the order of the derivative of the term it is attached to, i.e., $k = 0$ indicates the original quantities, $k = 1$ signifies the first order derivative, and so on. In Table-II, $\dot{x}$ and $\ddot{x}$ represent the first and second order derivatives of the quantity x, respectively.

B. Estimation of the Coefficients of Constitutive Equations

To obtain the value of the coefficients in (2) - (7) we form an overdetermined system of linear algebraic equations (LAEs) by substituting recorded stress and resistance data for each time-step. Solving this system of equations gives us the values of these coefficients. The generalized form of the system of LAEs is:

$$\begin{pmatrix} \boldsymbol{\Sigma} & \boldsymbol{\mathfrak{R}} \end{pmatrix}_{m\times n} \begin{pmatrix} \mathbf{p} \\ \mathbf{q} \end{pmatrix}_{n\times 1} = \boldsymbol{\sigma}_{m\times 1} \tag{8}$$

Bold font signifies a vector/matrix symbol. The matrix $\begin{pmatrix} \boldsymbol{\Sigma} & \boldsymbol{\mathfrak{R}} \end{pmatrix}$ consists of vectors of discrete values of the n terms on the left hand side, where $\boldsymbol{\Sigma}$ represents the stress derivative terms and $\boldsymbol{\mathfrak{R}}$ represents relative resistance and its derivatives. Hence, $m >> n$. $\begin{pmatrix} \mathbf{p} & \mathbf{q} \end{pmatrix}^{\mathrm{T}}$ represents the vector of coefficients for each equation, with the columns of the first matrix varying accordingly and $\boldsymbol{\sigma}$ is a vector of the recorded values of stress at each data-point.

In order to determine the values of $\begin{pmatrix} \mathbf{p} & \mathbf{q} \end{pmatrix}^{\mathrm{T}}$, we use the Moore-Penrose inverse, or pseudo-inverse of the matrix $\begin{pmatrix} \boldsymbol{\Sigma} & \boldsymbol{\mathfrak{R}} \end{pmatrix}$. Hence, the coefficients can be numerically determined by,

$$\begin{pmatrix} \mathbf{p} \\ \mathbf{q} \end{pmatrix} = \begin{pmatrix} \boldsymbol{\Sigma} & \boldsymbol{\mathfrak{R}} \end{pmatrix}^{\dagger} \boldsymbol{\sigma} \tag{9}$$

Where $\mathbf{A}^{\dagger}$ represents the pseudo-inverse of matrix $\mathbf{A}$, which is calculated as:

$$\mathbf{A}^{\dagger} = \mathbf{A}^{\mathrm{T}} \left(\mathbf{A}\mathbf{A}^{\mathrm{T}} \right)^{-1} \tag{10}$$

Using the values of the coefficients determined from (9), we solve (2) - (7) numerically, and compare the accuracy of each model for the two case-studies mentioned previously.

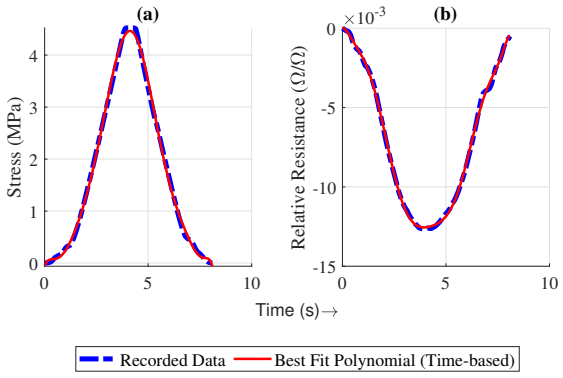

Fig. 4. Plot of Recorded values and their Best Fit Polynomials (a) Stress v/s Time (b) Relative Resistance v/s Time

IV. Results and Discussion

A. Recorded Stress and Resistance Plots

Figure 4 shows the values of stress and relative resistance over one test cycle, calculated from recorded data, and the plots of their respective best-fit polynomials. At the maximum engineering stress of ∼4.55 MPa and strain of ∼0.06, the corresponding relative resistance was -0.0126 (a change of about 20 mV). The best-fit polynomials of each quantity were used to regenerate a smooth set of data-points, to obtain the values of the derivatives of each quantity with respect to time.

B. Stress Prediction using Coefficients from complete cycle

Using (9), the values of the coefficients for each model were determined, as shown in Table-III. Figure 5 shows the comparison of stresses predicted by each model over the entire cycle. Apart from the 2-parameter Maxwell and the 4-parameter Burger models, the remaining predictions have similar profiles. However, the predictions still show a large difference from the original stress profile (here, 'original'

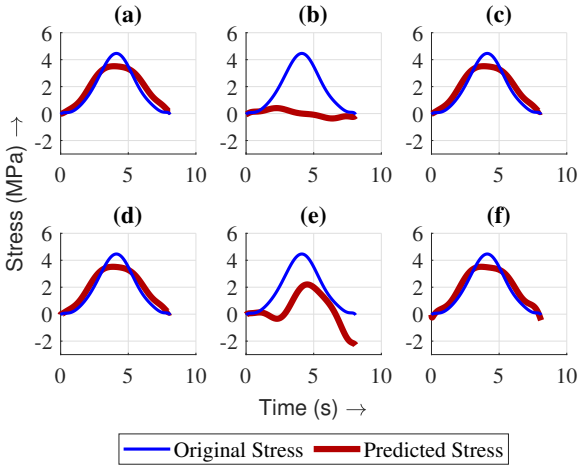

Fig. 5. Comparison of Predicted Stresses with coefficients calculated over a full cycle for (a) Hookean Elastic model (b) 2-Parameter Maxwell model (c) 2-Parameter Kelvin model (d) 3-Parameter Zener models (e) 4-Parameter Burger models (f) 4-Parameter Kelvin model

TABLE III

ESTIMATED MODEL COEFFICIENTS FOR DIFFERENT CASES

P	C	H	M	K	Z	B	GK2
F	p_0	1	1	1	1	1	1
	p_1	–	0.1574	–	0.0093	0.3312	0.0216
	p_2	–	–	–	–	0.8737	–
	q_0	-279.9	–	-279.9	-279.8	–	-276.2
	q_1	–	-69.6	-20.8	-23.7	-142.2	-27.5
	q_2	–	–	–	–	358.9	20.6
L	p_0	1	1	1	1	1	1
	p_1	–	2.6	–	0.24	2.5	0.2
	p_2	–	–	–	–	0.5	–
	q_0	-286.5	–	-330.5	-353.4	–	-353.1
	q_1	–	477.8	148.3	106.2	389.1	110.8
	q_2	–	–	–	–	-115.2	-3.7
U	p_0	1	1	1	1	1	1
	p_1	–	2.2	–	0.22	2.1	0.2
	p_2	–	–	–	–	0.2	–
	q_0	-273.9	–	-330.6	-353.4	–	-351.6
	q_1	–	-345.8	-207.8	-175.9	-300.4	-176.4
	q_2	–	–	–	–	3.7	2.9

Labels: P = Phases, C = Coefficients, H = Hooke, M = Maxwell, K = 2-Parameter Kelvin, Z = Zener, B = Burger, GK2 = 4-Parameter Kelvin (2 Loops), F = Full Cycle, L = Loading Phase, U = Unloading Phase

refers to the best-fit polynomial). It can be inferred that a generalized set of coefficients do not characterize the material behaviour correctly due to viscoelastic hysteresis, where the stress-strain behaviour differs in loading and unloading.

C. Stress Prediction using Phase-wise Coefficients

To account for the effects of viscoelastic hysteresis, model coefficients were determined separately for loading and unloading phases of the test-cycle. Observing the resistance

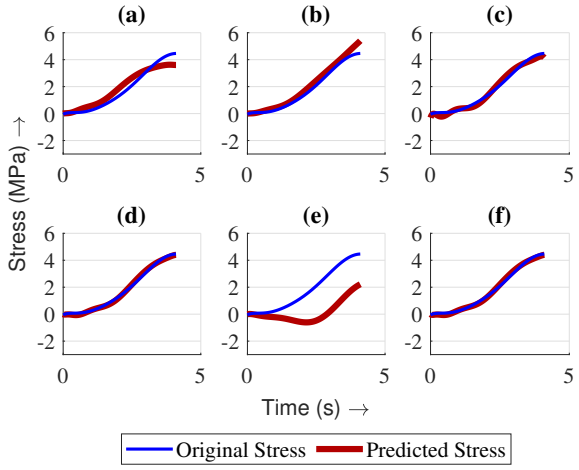

Fig. 6. Comparison of Predicted Stresses with coefficients calculated over the loading phase for (a) Hookean Elastic model (b) 2-Parameter Maxwell model (c) 2-Parameter Kelvin model (d) 3-Parameter Zener models (e) 4-Parameter Burger models (f) 4-Parameter Kelvin model

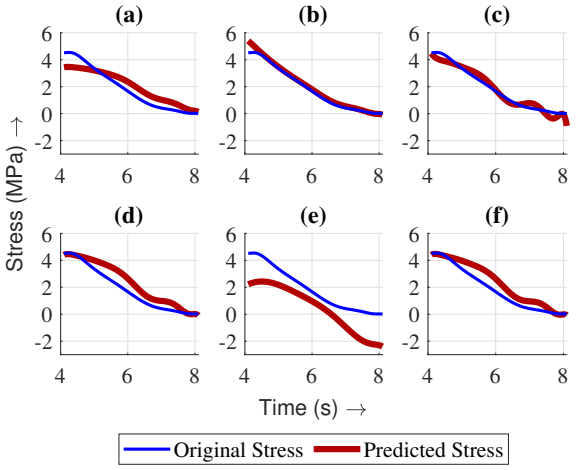

Fig. 7. Comparison of Predicted Stresses with coefficients calculated over the unloading phase for (a) Hookean Elastic model (b) 2-Parameter Maxwell model (c) 2-Parameter Kelvin model (d) 3-Parameter Zener models (e) 4-Parameter Burger models (f) 4-Parameter Kelvin model

plot in Fig. 4, the rate of change of relative resistance can be used to determine the phase of loading. When solving (2) - (7), the initial conditions for the loading phase are supplied by the original data, while those for the unloading phase are taken from end of the loading-phase predictions. It can be seen from Table-III, that there are significant differences between the values of the coefficients for loading and unloading phases.

Looking at Figs. 6 & 7, the predicted stress profiles appear much more accurate in the loading phase, compared to the unloading phase, especially for the Zener and Kelvin models. The prediction from Hooke's model does not show much change from the previous case, which can be reasonably justified by the values of it's model coefficient in both cases. The Maxwell model however, provides a much more accurate prediction, compared to the previous case. Table-IV gives the root mean square (RMS) errors between the predicted and original stresses. Compared to the errors observed from using full-cycle model coefficients, the error values for phase-wise coefficients are lesser overall. Both 2-parameter Kelvin and Maxwell models show the best overall prediction accuracy in this case. However, compared to the Maxwell model, the Kelvin model manages to better predict the decrease in the rate of loading before the change of phase. The

TABLE IV

RMS ERRORS OF STRESS PREDICTION MODELS

Model	Full Cycle	Loading	Unloading
1-Parameter Hooke	0.5295	0.4400	0.6072
2-Parameter Maxwell	2.3656	0.2966	0.1901
2-Parameter Kelvin	0.5245	0.1826	0.2883
3-Parameter Zener	0.5243	0.1235	0.6281
4-Parameter Burger	1.7308	1.9451	1.5243
4-Parameter Kelvin	0.5168	0.1241	0.6077

3-parameter Zener and 4-parameter Kelvin models have an especially high accuracy in the loading phase. They too, manage to predict the decrease of loading speed before direction change at the end of the loading phase. Burger's model shows the highest inaccuracy. Considering the fact that (6) is the only constitutive equation among the considered models with a second order stress derivative term, its solution consists of the exponential term with a sinusoidal coefficient: $\sin(1.106t + 1.296) \bullet e^{-0.2087t}$. Hence, it can be concluded that increasing the order of the constitutive model can lead to a rise in instability, even when the original dataset is used for prediction. For a real situation with uncertainties, using a higher order differential model can quickly lead to an unstable output. Hence, in further studies lower order models with variable model parameters that can be predicted with resistance or strain will be considered.

V. Conclusion and Future Scope

In this study, we have considered six resistive-viscoelastic rheological models, and shown the empirical determination of coefficients for their constitutive equations. To obtain the data for empirical calculations, a cuboidal conductive body was printed, with a cross-section of 100 mm^2 and subjected to compressive loading of about 450 N at a loading speed of 10 mm/min for one cycle. Owing to the sufficiently complex mechanical structure of the body (50% infill in the conductive part and four layers of solid fill at the top), empirically estimating the model coefficients was found to be the most practical approach. Using these coefficients, the various constitutive equations were solved to determine the value of stress over time, as predicted by each model. Two cases were considered: When the coefficients are estimated using values from the entire cycle and when they are determined phase-wise, i.e., the loading and unloading phases. Due to hysteresis in viscoelastic materials, determining coefficients separately for each phase gave a much more accurate output than using generalized coefficients. We also determined that using higher order models can lead to instabilities, as observed from the results of the 4-parameter Burger's model, due to the inclusion of exponential terms with sinusoidal coefficients in the solution.

Hence, through this study, it was determined that objects 3D-printed with conductive PLA display a change in resistance that is dependent on the load as well as rate of loading and its higher order transients. It was seen that 2 and 3-parameter models provide sufficient prediction accuracy for phase-wise prediction. This method can be easily used to determine the most applicable resistive-viscoelastic model for piezoresistive conductive polymers, in ranges where the strain and resistance follow linear laws. Future efforts will focus on obtaining a model to be used with real-time systems.

References

[1] I. Tirado-Garcia, D. Garcia-Gonzalez, S. Garzon-Hernandez, A. Rusinek, G. Robles, J. Martinez-Tarifa, and A. Arias, "Conductive 3D printed PLA composites: On the interplay of mechanical, electrical and thermal behaviours," *Composite Structures*, vol. 265, p. 113744, June 2021. [Online]. Available: https://linkinghub.elsevier.com/retrieve/pii/S0263822321002051

[2] I. Colombaro, R. Garra, A. Giusti, and F. Mainardi, "Scott-Blair models with time-varying viscosity," *Applied Mathematics Letters*, vol. 86, pp. 57–63, Dec. 2018. [Online]. Available: https://linkinghub.elsevier.com/retrieve/pii/S089396591830199X

[3] G. M. Kamath and N. M. Wereley, "A nonlinear viscoelastic - plastic model for electrorheological fluids," *Smart Materials and Structures*, vol. 6, no. 3, pp. 351–359, June 1997. [Online]. Available: https://iopscience.iop.org/article/10.1088/0964-1726/6/3/012

[4] M. Kalantari, J. Dargahi, J. Kvecses, M. G. Mardasi, and S. Nouri, "A New Approach for Modeling Piezoresistive Force Sensors Based on Semiconductive Polymer Composites," *IEEE/ASME Transactions on Mechatronics*, vol. 17, no. 3, pp. 572–581, June 2012. [Online]. Available: http://ieeexplore.ieee.org/document/5727954/

[5] S. Yong and K. Aw, "Modeling Electrical Resistance Behavior of Soft and Flexible Piezoresistive Sensors Based on Carbon-Black/Silicone Elastomer Composites," *Sensing and Imaging*, vol. 23, no. 1, p. 22, Dec. 2022. [Online]. Available: https://link.springer.com/10.1007/s11220-022-00392-4

[6] M. Wang, R. Gurunathan, K. Imasato, N. R. Geisendorfer, A. E. Jakus, J. Peng, R. N. Shah, M. Grayson, and G. J. Snyder, "A Percolation Model for Piezoresistivity in ConductorPolymer Composites," *Advanced Theory and Simulations*, vol. 2, no. 2, p. 1800125, Feb. 2019. [Online]. Available: https://onlinelibrary.wiley.com/doi/10.1002/adts.201800125

[7] D. Guo, X. Pan, Y. Xie, Y. Liu, and H. He, "Effects of service condition on the performance of conductive polymer composites for flexible strain sensors," *Sensors and Actuators A: Physical*, vol. 318, p. 112494, Feb. 2021. [Online]. Available: https://linkinghub.elsevier.com/retrieve/pii/S0924424720318094

[8] L. Paredes-Madrid, A. Matute, J. Bareo, C. Parra Vargas, and E. Gutierrez Velsquez, "Underlying Physics of Conductive Polymer Composites and Force Sensing Resistors (FSRs). A Study on Creep Response and Dynamic Loading," *Materials*, vol. 10, no. 11, p. 1334, Nov. 2017. [Online]. Available: http://www.mdpi.com/1996-1944/10/11/1334

[9] S. Garzon-Hernandez, A. Arias, and D. Garcia-Gonzalez, "A continuum constitutive model for FDM 3D printed thermoplastics," *Composites Part B: Engineering*, vol. 201, p. 108373, Nov. 2020. [Online]. Available: https://linkinghub.elsevier.com/retrieve/pii/S1359836820334193

[10] Q. Mu, J. Wang, and X. Kuang, "Modeling the resistive viscoelasticity of conductive polymer composites for sensor usage," *Soft Matter*, vol. 19, no. 5, pp. 1025–1033, 2023. [Online]. Available: https://xlink.rsc.org/?DOI=D2SM01463G

[11] Y. Gao, Q. Li, A. Dong, F. Wang, and X. Wang, "Characterizing the Resistance Relaxation of the Fabric-based Resistive Sensors Based on an Electro-mechanical Model," *Sensors and Actuators A: Physical*, vol. 310, p. 112041, Aug. 2020. [Online]. Available: https://linkinghub.elsevier.com/retrieve/pii/S0924424720304702

[12] S. Kouchakzadeh and K. Narooei, "Simulation of piezoresistance and deformation behavior of a flexible 3D printed sensor considering the nonlinear mechanical behavior of materials," *Sensors and Actuators A: Physical*, vol. 332, p. 113214, Dec. 2021. [Online]. Available: https://linkinghub.elsevier.com/retrieve/pii/S0924424721006774

[13] A. Kadival, J. Mitra, M. Kaushal, and R. Machavaram, "Prediction of Viscoelastic Properties of Peanut-based 3D Printable Food ink," *Journal of Texture Studies*, vol. 55, no. 1, p. e12817, Feb. 2024. [Online]. Available: https://onlinelibrary.wiley.com/doi/10.1111/jtxs.12817

[14] M. Karabal and A. Yildiz, "Creep resistance enhancement and modeling of 3D printed Polyetherimide/carbon black composites," *Composite Structures*, vol. 345, p. 118398, Oct. 2024. [Online]. Available: https://linkinghub.elsevier.com/retrieve/pii/S0263822324005269

[15] Protopasta, "Conductive PLA." [Online]. Available: https://proto-pasta.com/pages/conductive-pla

[16] S. Shang, Y. Yue, and X. Wang, "Piezoresistive strain sensing of carbon black /silicone composites above percolation threshold," *Review of Scientific Instruments*, vol. 87, no. 12, p. 123910, Dec. 2016. [Online]. Available: https://pubs.aip.org/rsi/article/87/12/123910/916719/Piezoresistive-strain-sensing-of-carbon-black

[17] H. F. Brinson and L. C. Brinson, *Polymer Engineering Science and Viscoelasticity: An Introduction*. Boston, MA: Springer US, 2015. [Online]. Available: https://link.springer.com/10.1007/978-1-4899-7485-3